Integrated Configuration and Control Strategy for PV Generation in Railway Traction Power Supply Systems

Peng Cheng, *Member*, *IEEE*, *Member*, *CSEE*, Huiwen Kong, Chao Wu, *Member*, *IEEE*, and Jing Ma, *Senior Member*, *IEEE*

***Abstract*—Recently, electric railways have experienced a rapid development causing an increasing power demand. Due to the flexible installation available at trackside land along railways, photovoltaic (PV) generation is suggested as an extension to the traction power supply system (TPSS) in railways. First, this paper proposes a three-phase integrated configuration for PV generation connected to a two-phase traction network and the on-site consumption of solar resources alongside railways. In this configuration, another inverse V/V transformer is used to maintain a balanced three-phase low voltage (LV) AC bus from a two-phase traction network. It is more convenient for accessing PV generation units. Then, in order to mitigate the negative sequence currents caused by electric trains, an individual phase current (IPC) control strategy for PV converters is developed for power quality improvement. It can not only supply the locomotive with asymmetrical currents, but also provide feedback to the grid through symmetrical currents. All the implementation and calculations are conducted in the three-phase stationary reference frame without any sequence extracting and power compensations. Finally, simulation results are presented to validate the effectiveness of the proposed IPC control strategy.**

***Index Terms*—Current control, individual phase current (IPC), photovoltaic (PV) converter, railway traction network.**

NOMENCLATURE

k_1, k_2, k_3	Ratios of V/V, inverse V/V and isolated transformers.
$u_{\rm A}, u_{\rm B}, u_{\rm C}$	Three-phase high voltages.
u_α, u_β	Traction voltage.
$u_{\rm ga}, u_{\rm gb}, u_{\rm gc}$	Three-phase voltages of LV ac bus.
$u_{\rm ca}, u_{\rm cb}, u_{\rm cc}$	Three-phase converter voltages.
$i_{\rm A}, i_{\rm B}, i_{\rm C}$	Three-phase currents in HV side.
i_α, i_β	Traction current of α and β-arm.
$i_{C\alpha}, i_{C\beta}$	Injected currents of PV generation unit in α- and β-arm.
$i_{\rm L\alpha}, i_{\rm L\beta}$	Locomotive current of α- and β-arm.
$i_{\rm ga}, i_{\rm gb}, i_{\rm gc}$	Three-phase currents of LV ac bus.
$i_{\rm ca}, i_{\rm cb}, i_{\rm cc}$	Three-phase converter currents.
$P_{\rm cap}, P_{\rm dc}$	The capacitor power, and the active power delivered to the dc link.
$V_{\rm dc}, C$	DC link voltage and capacitance.
ω	Grid angular frequency.
$P_{\rm cref}, Q_{\rm cref}$	Converter active and reactive power reference.
$v_{\rm a}, v_{\rm b}, v_{\rm c}$	Converter modulated voltage.
$v'_{\rm a}, v'_{\rm b}, v'_{\rm c}$	Converter current controller output.
$u_{\rm cac}, u_{\rm cbc}, u_{\rm cab}$	Converter line voltage.
$u_{\rm cac\_pu}, u_{\rm cbc\_pu}, u_{\rm cab\_pu}$	Per-unit values of converter line voltage.
$i_{\rm caref}, i_{\rm cbref}, i_{\rm ccref}$	Converter current references.
$i_{\rm caref\_pu}, i_{\rm cbref\_pu}, i_{\rm ccref\_pu}$	Per-unit values of converter current references.

Manuscript received July 21, 2020; revised August 24, 2020; accepted October 13, 2020. Date of online publication November 20, 2020; date of current version February 23, 2022. This work was supported in part by the National Natural Science Foundation of China (51807182).

P. Cheng (ORCID: https://orcid.org/0000-0001-8932-2011), H. W. Kong and J. Ma are with China Institute of Energy and Transportation Integrated Development, North China Electric Power University, Beijing 102206, China.

C. Wu (corresponding author, email: wuchao@sjtu.edu.cn, ORCID: https://orcid.org/0000-0003-0181-4738) is with Department of Electrical Engineering, Shanghai Jiao Tong University, Shanghai, 200240, China; and also with department of energy, Aalborg University, Aalborg 9220, Denmark.

DOI: 10.17775/CSEEJPES.2020.03480

I. INTRODUCTION

RECENTLY, rail transportation has achieved a rapid development due to its advantages, including lower carbon emissions and higher efficiencies [1], [2]. The International Energy Agency (IEA) forecasts that the global rail network will expand from 1.6 to 2.1 million track-kilometers during 2016 to 2050, a 26% increase for these years [3]. The development of the rail network will cause a rapid increase in energy demand, especially in the form of electricity, primarily due to growing traffic conditions and faster trains. The upgrading of the traction power supply in rail transportation is essential through adding new connections from more sources. It is reported that by 2050, the share of renewable power will be up to 86% in the power sector [4]. As a result, renewable power is expected to play a greater role in the railway traction power supply system (TPSS).

The integration of renewable power in the railway TPSS is anticipated to support the increasing electricity demand. Among the various types of renewable energy, photovoltaic (PV) generation is more suitable for this integrated application, which is primary because there is more available space at station rooftops and trackside land [5], [6]. Nowadays, rail

2096-0042 © 2020 CSEE

operators and infrastructure managers are increasingly taking advantage of their own land space to operate PV generation with a reduced dependence on the main grid. For example, in England, a 30 kW PV array is connected to an ancillary transformer in the traction system to power lights and signaling equipment [7]. In 2011, Japan Rail-East operated the first installed 453 kW PV generation above the entire platform at Tokyo Station and then in 2014 began using a 1050 kW PV generation system inside the Keiyo Rolling Stock Center [8]. The initial trials confirm that there is a strong potential for PV generation-integrated railway electrification with technology progress and cost reduction. The commonest solution for integrating PV generation in railway feeder stations is to connect PV generation to the high-voltage side (110 kV or 220 kV) of the traction station with no modification in the railway traction network [9], [10]. Under such cases, a high-radio transformer is needed due to the low voltage of PV converters and panels. Thus, the connection to the traction side for a lower connected voltage (27.5 kV) is suggested with less voltage rating and less infrastructures. For the connection to the traction network, a single-phase-based configuration is developed in [11], [12], where two AC ports of the back-to-back single-phase converter is connected to two step-down transformers, respectively. In addition, a DC/DC converter is connected to a common DC link for providing one DC port to connect to the PV panels. Thus, a three-port converter, consisting two AC ports and one DC port, is used in this configuration with a complex control implementation. Due to no common AC bus, it is difficult to integrate more converters at the connection point. Meanwhile, for larger power delivery, a three-phase integrated configuration and power converter are preferred. Consequently, a three-phase integrated configuration for PV generation in railway TPSSs needs further investigations.

Since an electrified train is a single-phase locomotive load, PV converters are required to inject unbalanced current, containing both positive and negative sequence currents, to supply single-phase locomotive loads. Various approaches are proposed to enhance the tracking capability of unbalanced currents, which are categorized into two groups. One is the rotating reference frame-based solution. It is normally done by implementing a dual-sequence current controller consisting of dual proportional integral (PI) controllers or PI plus resonant (PIR) controllers [13], [14]. The other one is the stationary reference frame-based solution. Since the positive and negative sequence currents in the stationary reference frame is of the same frequency, various stationary controllers can be used to regulate dual sequence currents, e.g., hysteresis [15], sliding mode [16], predictive [17] and proportional plus resonant (PR) [18] controllers. With these aforementioned controllers, the current reference can be well tracked with zero steady errors. Thus, the current reference generation would be a crucial aspect, which determines the grid-connected performance of the converter. Several power-characteristic-oriented current references are fully designed on the basis of instantaneous power theory [19]–[22], which are aimed at directly regulating the oscillating powers. These all have specific control targets, such as the quality of injected currents [19], mitigation of DC voltage ripples [20], and achievement of a constant active and/or reactive power provision [21], [22]. For facilitating multiple targets with various current references, flexible positive and negative sequence control is proposed on dual sequence voltages in [23], [24]. By this means, several aforementioned targets can be flexibly accommodated based on two independent adjustable parameters. Common to all these methods is that the control strategies of positive and negative sequence currents are usually considered only for a three-phase load, which are not suitable for powering electrified trains, that are a type of single-phase load. Thus, the control strategy of a PV converter for powering a single-phase locomotive load needs be studied.

This paper presents a three-phase integrated configuration and individual phase current (IPC) control strategy for PV generation in railway TPSSs. The integrated configuration is developed with a low voltage (LV) three-phase AC bus, which is more convenient for more access. The IPC control strategy for flexible injection between asymmetrical and symmetrical current is proposed. All the calculations and implementation are conducted in the stationary reference frame without any sequential extraction and power compensation. The remainder of this paper is structured as follows. Section II describes the three-phase integrated configuration of PV generation in railway TPSSs. In Section III, the IPC control strategy is designed in detail. Then, Section IV includes the simulation validation of the proposed IPC control strategy. Finally, Section V summarizes the conclusions.

II. Integrated Configuration

In this section, a 25 kV, 50 Hz electrification system is given as an example, which is connected to a high-voltage utility grid at 110 kV, called the high voltage (HV) side. In practice, a V/V transformer is widely used for the simple structure and the high-capacity utilization to step down the three-phase high voltage into two-phase traction voltage, called α- and β-arm. Since PV generations operate typically at low voltage, it is suggested to be connected to the traction arms at the front end of the catenary network. Therefore, in this section, two different integrated configurations are discussed and compared.

Figure 1 shows a single-phase integrated configuration of a PV generation into railway TPSSs. Two single-phase transformers are used to step down the traction voltage 27.5 kV to 10(6) kV, called the LV side. Then, PV generation units are connected to the secondary side of single-phase transformers through low voltage power cables. The single-phase PV generation consists of two single-phase isolated transformers, a two single-phase DC/AC converter and one DC/DC converter with a common DC link. The former is used to deliver the active power to the selected traction arm with the locomotives, while the latter is used to track and deliver the maximum power of the PV panels to the common DC-link. However, since there are two AC output ports and a common DC link for three converters, a coordinated control is needed for maintaining constant DC voltage and power delivery. When there is a locomotive load on one traction arm, the power is delivered through the corresponding converter connected to the specific traction arm. However, without no locomotive load on the

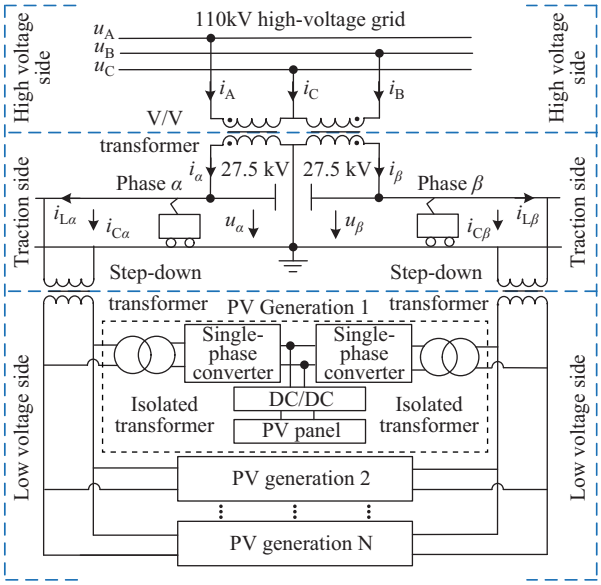


Fig. 1. Single-phase integrated configuration of PV generation.

traction arms, the PV power is delivered to the grid by one or two single-phase converters with unbalanced current and oscillating power in the three-phase system.

For this drawback, Fig. 2 develops a three-phase integrated configuration of PV generation into railway TPSSs. In the proposed connection, another inverse V/V transformer is used to not only step down 27.5 kV traction voltage to 10 (6) kV low voltage but also converts two phase voltage in the traction network to three phase voltage in the LV side. By this means, an LV AC bus is provided for the grid connection of the conventional three-phase PV generation, which is made up of a Y/Y isolated transformer, a three-phase converter, a

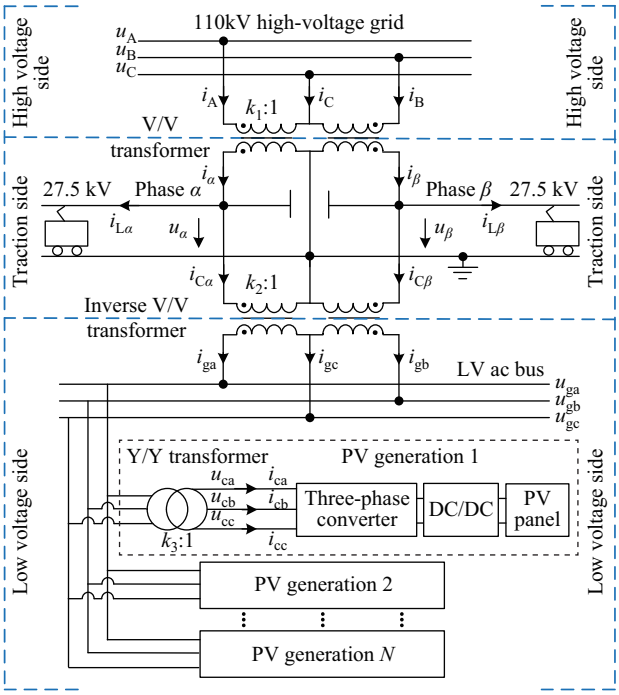


Fig. 2. Three-phase integrated configuration of PV generation.

DC/DC converter and PV panels.

According to Fig. 2, the voltage relationship of the HV side, the traction side and the LV side is presented as,

$$\begin{bmatrix} u_\alpha \\ u_\beta \end{bmatrix} = \frac{1}{k_1}\begin{bmatrix} 1 & 0 & -1 \\ 0 & 1 & -1 \end{bmatrix}\begin{bmatrix} u_{\mathrm{A}} \\ u_{\mathrm{B}} \\ u_{\mathrm{C}} \end{bmatrix} \tag{1}$$

$$\begin{bmatrix} u_\alpha \\ u_\beta \end{bmatrix} = k_2\begin{bmatrix} 1 & 0 & -1 \\ 0 & 1 & -1 \end{bmatrix}\begin{bmatrix} u_{\mathrm{ga}} \\ u_{\mathrm{gb}} \\ u_{\mathrm{gc}} \end{bmatrix} = k_2k_3\begin{bmatrix} 1 & 0 & -1 \\ 0 & 1 & -1 \end{bmatrix}\begin{bmatrix} u_{\mathrm{ca}} \\ u_{\mathrm{cb}} \\ u_{\mathrm{cc}} \end{bmatrix} \tag{2}$$

where k_1, k_2 and k_3 are the ratios of V/V, inverse V/V and Y/Y isolated transformers, u_{A}, u_{B}, u_{C} are three-phase high voltages, u_α, u_β are the traction voltages, u_{ga}, u_{gb}, u_{gc} are the three-phase voltages of the LV AC bus, u_{ca}, u_{cb}, u_{cc} are the three-phase converter voltages, respectively.

It is noted that since a Y/Y isolated transformer is used in the PV generation unit, there would be no zero-sequence currents on the LV side. Thus, the secondary-side voltage of the inverse V/V transformer has no zero-sequence voltage. Meanwhile, it is assumed that the high voltage is balanced with the no zero-sequence component for simple analysis. Then, the following equation can be obtained by,

$$\begin{cases} u_{\mathrm{ca}} + u_{\mathrm{cb}} + u_{\mathrm{cc}} = 0 \\ u_{\mathrm{A}} + u_{\mathrm{B}} + u_{\mathrm{C}} = 0 \end{cases} \tag{3}$$

Based on (1), (2) and (3), the relationship of high voltages and converter voltages is expressed as,

$$\begin{bmatrix} u_{\mathrm{ca}} \\ u_{\mathrm{cb}} \\ u_{\mathrm{cc}} \end{bmatrix} = \frac{1}{k_1k_2k_3}\begin{bmatrix} u_{\mathrm{A}} \\ u_{\mathrm{B}} \\ u_{\mathrm{C}} \end{bmatrix} \tag{4}$$

As seen from (4), the three-phase converter voltage is proportional to the high voltage. Since the high voltages are assumed to be balanced with no negative sequence voltage, the converter voltage would also be balanced.

Then, focused on the current relationship of the HV side, the traction side, the LV side and the converter side, the following equations are obtained as,

$$\begin{bmatrix} i_{\mathrm{A}} \\ i_{\mathrm{B}} \\ i_{\mathrm{C}} \end{bmatrix} = \frac{1}{k_1}\begin{bmatrix} 1 & 0 \\ 0 & 1 \\ -1 & -1 \end{bmatrix}\begin{bmatrix} i_\alpha \\ i_\beta \end{bmatrix} \tag{5}$$

$$\begin{bmatrix} i_{\mathrm{C}\alpha} \\ i_{\mathrm{C}\beta} \end{bmatrix} = \frac{1}{k_2}\begin{bmatrix} 1 & 0 & 0 \\ 0 & 1 & 0 \end{bmatrix}\begin{bmatrix} i_{\mathrm{ga}} \\ i_{\mathrm{gb}} \\ i_{\mathrm{gc}} \end{bmatrix} = \frac{1}{k_2k_3}\begin{bmatrix} 1 & 0 & 0 \\ 0 & 1 & 0 \end{bmatrix}\begin{bmatrix} i_{\mathrm{ca}} \\ i_{\mathrm{cb}} \\ i_{\mathrm{cc}} \end{bmatrix} \tag{6}$$

where i_{A}, i_{B}, i_{C} are the three-phase currents on the HV side, i_{ga}, i_{gb}, i_{gc} are three-phase currents of the LV AC bus, i_{ca}, i_{cb}, i_{cc} are three-phase converter currents, i_α, i_β are traction arm currents, $i_{C\alpha}$ and $i_{C\beta}$ are injected currents from the PV generation units into the α and β traction arms, respectively.

As shown in Fig. 2, the traction arm currents consist of both the locomotive currents and injected currents from the PV generation units, which can be expressed as,

$$\begin{bmatrix} i_\alpha \\ i_\beta \end{bmatrix} = \begin{bmatrix} i_{\mathrm{L}\alpha} \\ i_{\mathrm{L}\beta} \end{bmatrix} + \begin{bmatrix} i_{\mathrm{C}\alpha} \\ i_{\mathrm{C}\beta} \end{bmatrix} \tag{7}$$

where $i_{L\alpha}$, $i_{L\beta}$ are locomotive currents in the α- and β-arm, respectively.

According to (5), (6) and (7), the injected current of the utility grid is expressed in terms of the traction load current and LV AC bus current as,

$$\begin{bmatrix} i_A \\ i_B \\ i_C \end{bmatrix} = \frac{1}{k_1}\begin{bmatrix} 1 & 0 \\ 0 & 1 \\ -1 & -1 \end{bmatrix}\begin{bmatrix} i_{L\alpha} \\ i_{L\beta} \end{bmatrix} + \frac{1}{k_1 k_2 k_3}\begin{bmatrix} i_{ca} \\ i_{cb} \\ i_{cc} \end{bmatrix} \tag{8}$$

Based on (4) and (8), Fig. 3 presents the phasor diagram of the three-phase integrated configuration of the PV generation in TPSS. As seen, if proper current is injected from the three-phase converters, the PV generation units can serve as a compensator for power quality improvement.

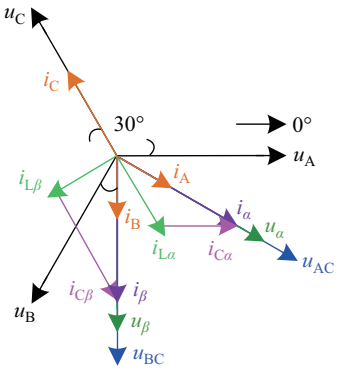


Fig. 3. Phasor diagram of three-phase configuration.

Compared to the single-phase integrated configuration in Fig. 1, the three-phase integrated configuration provides a three-phase LV AC bus for the connection of the PV generation units. Thus, the conventional three phase converter can still be used in this integrated configuration with a simpler implementation and a concentrated integration. When there is no locomotive load, the converter can simply inject a three-phase balanced current to guarantee balanced current and constant power on the high voltage side. By this means, the unbalanced current and oscillating power in the three phase system caused by the single-phase converter are avoided. When there is a locomotive load on one traction arm, the proper current injection is needed to deliver the total active power to the locomotive load for power quality improvement, which will be discussed in the next section.

III. IPC Strategy

A. DC-link Voltage Control

Figure 4 shows a simplified single-line diagram circuit of a grid-connected PV converter, where the connection point refers to the secondary side of the Y/Y isolated transformer. Since a DC/DC converter works as a maximum power point tracking (MPPT), the PV power injected into the DC-link is constant. By neglecting the converter losses, the DC-link capacitor power is expressed as,

$$P_{cap} = V_{dc} C \frac{dV_{dc}}{dt} = P_{dc} + P_c \tag{9}$$

where P_{cap}, P_c and P_{dc} are the capacitor power, the converter active power and the injected power from the front-end DC/DC converter, V_{dc} and C are the DC-link voltage and capacitance, respectively.

It is noted that the injected power from the front-end DC/DC converter is a perturbation term for maintaining the constant DC-link voltage, which is usually ignored in the control system as indicated in [20], [21]. Consequently, in order to maintain the constant DC-link voltage, the active power reference of the converter can be simply set as,

$$P_{cref} = P_{cap} = V_{dc} i_{cap} \tag{10}$$

where i_{cap} refers to the capacitor current, which is expressed as,

$$i_{cap} = C\frac{dV_{dc}}{dt} = \left(k_{vp} + \frac{k_{vi}}{s}\right)(V_{dcref} - V_{dc}) \tag{11}$$

where V_{dcref} is the reference of the DC-link voltage, k_{vp} and k_{vi} are the proportional and integral parameters, respectively.

As seen, the DC-link voltage controller can maintain the constant DC voltage and then produce the active power reference P_{cref} for the current control. In addition, the PV converter is usually controlled at the unity power factor and then the reactive power reference is set as zero, i.e. $Q_{cref} = 0$.

B. Current Control

It is noted that, the current of each phase has an obvious and direct correspondence to load current in uneven load conditions, but similar correspondence cannot be found in the stationary $\alpha\beta$-axis and synchronous dq-axis currents. Since an electrified train is a type of single-phase locomotive load, individual phase current is a more preferred method to be controlled for directly regulating the active power injected through specific phases.

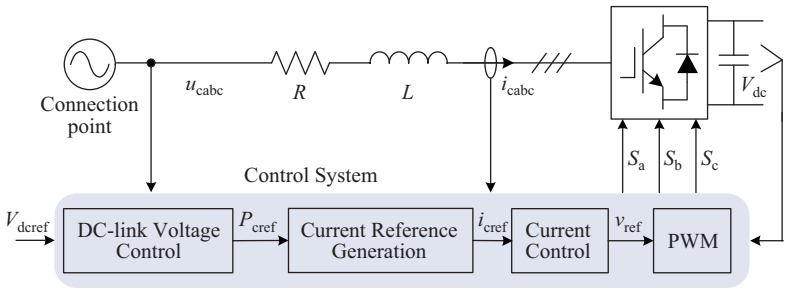


Fig. 4. Simplified single-line diagram circuit of the converter.

For converters, the dynamics between the output voltage v_{abc}, the grid voltage u_{cabc} and the output current i_{cabc} of each phase can be expressed as,

$$L\frac{\mathrm{d}}{\mathrm{d}t}\begin{bmatrix} i_{\text{ca}} \\ i_{\text{cb}} \\ i_{\text{cc}} \end{bmatrix} = \begin{bmatrix} u_{\text{ca}} \\ u_{\text{cb}} \\ u_{\text{cc}} \end{bmatrix} - R\begin{bmatrix} i_{\text{ca}} \\ i_{\text{cb}} \\ i_{\text{cc}} \end{bmatrix} - \begin{bmatrix} v_{\text{a}} \\ v_{\text{b}} \\ v_{\text{c}} \end{bmatrix} \tag{12}$$

where v_{abc}, i_{cabc} and u_{cabc} are the output phase voltages, the output phase currents and the grid phase voltages, L and R refer to the filter inductance and resistance, respectively.

Then, the modulated voltage v_{a}, v_{b} and v_{c} of each phase can be represented in the stationary reference frame as,

$$\begin{bmatrix} v_{\text{a}} \\ v_{\text{b}} \\ v_{\text{c}} \end{bmatrix} = \begin{bmatrix} u_{\text{ca}} \\ u_{\text{cb}} \\ u_{\text{cc}} \end{bmatrix} - R\begin{bmatrix} i_{\text{ca}} \\ i_{\text{cb}} \\ i_{\text{cc}} \end{bmatrix} - \begin{bmatrix} v'_{\text{a}} \\ v'_{\text{b}} \\ v'_{\text{c}} \end{bmatrix} \tag{13}$$

where v'_{a}, v'_{b} and v'_{c} are the outputs of the current controller,

$$\begin{bmatrix} v'_{\text{a}} \\ v'_{\text{b}} \\ v'_{\text{c}} \end{bmatrix} = G(s)\begin{bmatrix} i_{\text{caref}} - i_{\text{ca}} \\ i_{\text{cbref}} - i_{\text{cb}} \\ i_{\text{ccref}} - i_{\text{cc}} \end{bmatrix} \tag{14}$$

where i_{aref}, i_{bref} and i_{cref} are the current references in phase a, b and c, $G(s)$ is the transfer function of the current controller, respectively.

However, since the current references in (14) are AC signals for each phase, and the power reference in (11) is constant for three phases, they cannot be directly used as the current references. In addition, for locomotive loads, the active power is needed to be delivered via the specific two wires instead of three wires. Thus, the lack of the current reference generation is the main obstacle for three-phase converters to deliver active power into the traction side.

C. Current Reference Generation

As shown in Fig. 4, the outer DC voltage control loop and the inner current control loop are cascaded through the current reference generation, which is used to produce the current reference of the AC signals on the basis of the power reference of the DC signals. Especially for both symmetrical and asymmetrical current injections, more investigations need to be conducted on the current reference generation.

Based on instantaneous power theory, the active and reactive powers in the terms of converter voltages and currents of each phase can be obtained by,

$$\begin{cases} P_{\text{c}} = u_{\text{ca}}i_{\text{ca}} + u_{\text{cb}}i_{\text{cb}} + u_{\text{cc}}i_{\text{cc}} \\ Q_{\text{c}} = (u_{\text{cbc}}i_{\text{a}} + u_{\text{cac}}i_{\text{b}} + u_{\text{cab}}i_{\text{c}})/\sqrt{3} \end{cases} \tag{15}$$

where u_{cbc}, u_{cac}, u_{cab} are the line voltages between phase b and c, phase a and c, and phase a and b.

The converter is aiming at delivering the maximum active power to the locomotive load through specific phases. It is assumed that the locomotive is on α arm and no locomotive is on β arm, called Mode I. Based on Fig. 2, the active power should be delivered by phase a and phase c and the current of phase b is controlled to be zero. Thus, the currents of each phase in the stationary reference frame can be obtained by,

$$i_{\text{ca}} = -i_{\text{cc}}, i_{\text{cb}} = 0 \tag{16}$$

According to (16), equation (15) can be simplified as,

$$\begin{cases} P_{\text{c}} = (u_{\text{ca}} - u_{\text{cc}})i_{\text{ca}} = u_{\text{cac}}i_{\text{ca}} \\ Q_{\text{c}} = \sqrt{3}u_{\text{cb}}i_{\text{ca}} \end{cases} \tag{17}$$

where u_{cac} is the converter line voltage between phase a and c.

Since electrified trains are almost always equipped with PWM-based front-end rectifiers, they can operate in unity power factor mode. Thus, PV generation can still maintain unity power factor operation without a reactive power provision. Due to delivering only active power, the phase angle of the injected current must be in accordance with that of the line voltage, while its amplitude is determined by the active power from the DC-link to AC side.

$$i_{\text{ca}} = I_{\text{cref}}\frac{u_{\text{cac}}}{\sqrt{3}U_{\text{cm}}} \tag{18}$$

where I_{cref} is the amplitude of the converter current reference, U_{cm} is the amplitude of the converter rated phase voltage.

Assuming that the phase angle of the phase voltage u_{ca} is set at 0°, the line voltage u_{cac} is 30° lagging from the phase voltage u_{ca}. Consequently, the delivered active power can be calculated by,

$$\begin{aligned} P_{\text{c}} &= u_{\text{cac}}I_{\text{cref}}\frac{u_{\text{cac}}}{\sqrt{3}U_{\text{cm}}} = \sqrt{3}U_{\text{cm}}I_{\text{cref}}\sin^2(\omega t - 30^\circ) \\ &= \sqrt{3}U_{\text{cm}}I_{\text{cref}}\frac{1-\cos(2\omega t - 60^\circ)}{2} \end{aligned} \tag{19}$$

where ω is the grid angular frequency.

As seen, since the converter currents and voltages are all with a grid frequency, there would inevitably be twice the grid frequency pulsations in the active power, which are typical power features of single-phase AC systems. However, for maintaining a constant DC-link voltage, the average active power in (19) must track the average active power produced by the DC voltage controller. As a result, the amplitude of the converter current reference is obtained by,

$$I_{\text{cref}} = \frac{P_{\text{cref}}}{\sqrt{3}U_{\text{cm}}/2} \tag{20}$$

Based on (16), (18) and (20), the converter current reference of each phase can be obtained as,

$$\begin{cases} i_{\text{caref}} = \dfrac{P_{\text{cref}}}{\sqrt{3}U_{\text{cm}}^2/2}u_{\text{cac}} \\ i_{\text{cbref}} = 0 \\ i_{\text{ccref}} = -\dfrac{P_{\text{cref}}}{\sqrt{3}U_{\text{cm}}^2/2}u_{\text{cac}} \end{cases} \tag{21}$$

where i_{caref}, i_{cbref}, i_{ccref} is the amplitude of the converter current references of phases a, b and c.

In a per-unit system, the base values of voltage and current are set at the amplitudes of the rated phase voltage and phase current, respectively. Then, the power base value is obtained by,

$$\begin{cases} U_{\text{b}} = U_{\text{cm}}, I_{\text{b}} = I_{\text{cm}} \\ P_{\text{b}} = 3\dfrac{U_{\text{b}}}{\sqrt{2}}\dfrac{I_{\text{b}}}{\sqrt{2}} = 1.5U_{\text{cm}}I_{\text{cm}} = P_{\text{rated}} \end{cases} \tag{22}$$

where $I_{\rm cm}$ is the amplitude of rated phase current, $U_{\rm b}$, $I_{\rm b}$ and $P_{\rm b}$ are the base values of the voltage, current and power in a per-unit system, respectively.

Then, the amplitude of the current reference in (20) can be converted into per-unit value as,

$$I_{\rm cref\_pu} = \sqrt{3} P_{\rm cref\_pu} \tag{23}$$

where $P_{\rm cref\_pu}$ and $I_{\rm cref\_pu}$ are the per-unit values of active power and current reference amplitude, respectively.

Thus, the current reference of each phase in the per-unit system can be obtained as,

$$\begin{cases} i_{\rm caref\_pu} = P_{\rm cref\_pu} u_{\rm cac\_pu} \\ i_{\rm cbref\_pu} = 0 \\ i_{\rm ccref\_pu} = -P_{\rm cref\_pu} u_{\rm cac\_pu} \end{cases} \tag{24}$$

where $i_{\rm caref\_pu}$, $i_{\rm cbref\_pu}$, and $i_{\rm ccref\_pu}$ are the per-unit values of phase current reference, $u_{\rm cac\_pu}$ is the pre-unit values of line voltage between phase a and c, respectively.

As seen from (24), taking phase a as an example, the amplitude of the current reference is equal to the active power reference in a per-unit system. In addition, the phase angle of the current reference is the same as that of the line voltage between phase a and c.

When the locomotive load is on β arm, the active power should be delivered by phase b and c and the current of phase a is controlled to be zero, which is called Mode II. Based on the previous analysis, the converter current reference can be similarly obtained as,

$$\begin{cases} i_{\rm caref\_pu} = 0 \\ i_{\rm cbref\_pu} = P_{\rm cref\_pu} u_{\rm cbc\_pu} \\ i_{\rm ccref\_pu} = -P_{\rm cref\_pu} u_{\rm cbc\_pu} \end{cases} \tag{25}$$

where $u_{\rm cbc\_pu}$ is the pre-unit values of the converter line voltage between phase b and c.

When no locomotive load is on traction arms, called Mode III, the PV converter is required to inject three-phase balanced current with the unity-power-factor operation. For the PV converter, the amplitudes of each phase current reference are equal to each other. In addition, the phase angle of each phase current reference is in accordance with that of the corresponding phase voltage.

$$i_{\rm c}x = I_{\rm cbal} \frac{u_{\rm c}x}{U_{\rm cm}} \tag{26}$$

where $x =$ a, b and c refer to phases a, b and c, $i_{\rm c}x$ and $u_{\rm c}x$ are the converter current and voltage of phase x, $I_{\rm cbal}$ is the amplitude of the converter current, respectively.

Based on (15), the amplitude of the converter current is obtained by,

$$I_{\rm cbal} = \frac{P_{\rm cref}}{3U_{\rm cm}/2} \tag{27}$$

In the per-unit system, (27) can be rewritten as

$$I_{\rm cbal\_pu} = P_{\rm cref\_pu} \tag{28}$$

where $I_{\rm cbal\_pu}$ is the per-unit value of the phase current amplitude.

Then, based on (26), the current reference in the per-unit system is obtained as,

$$i_{\rm c}x_{\rm ref\_pu} = P_{\rm cref\_pu} u_{\rm c}x_{\rm \_pu} \tag{29}$$

where $i_{\rm c}x_{\rm ref\_pu}$ is the per-unit value of the current reference of phase x, $u_{\rm c}x_{\rm \_pu}$ is the per-unit value of voltage of phase x, respectively.

According to (24), (25) and (29), the current reference is generated for delivering maximum active power to the traction side. Based on the power of each traction arm, i.e., $P_{{\rm L}\alpha}$ and $P_{{\rm L}\beta}$, it is easy to distinguish the traction arm being powered and operating in the proper mode. In Mode I/II, since the converter delivers all the active power to the single-phase locomotive load, the negative sequence current caused by the locomotive load can be reduced. In Mode III, the converter injects balanced current into the grid without negative sequence current, which can achieve the balanced current and constant power in the three-phase HV side.

D. System Implementation

s analyzed previously, among various stationary controllers, the PR controller has been widely used due to its sufficient amplitude gain at operating frequency and simple implementation. In practice, a cutoff frequency $\omega_{\rm c} =$ 5–20 rad/s is introduced as a damping to guarantee the stable operation over a frequency variation range around the nominal grid angular frequency. Thus, the complete transfer function of the adopted current controller in (14) is given as,

$$G(s) = k_{\rm ip} + \frac{k_{\rm ir} 2\omega_{\rm c} s}{s^2 + 2\omega_{\rm c} s + \omega^2} \tag{30}$$

where $k_{\rm ip}$ and $k_{\rm ir}$ are the proportional and integral parameters, $\omega = 100\ \pi$ rad/s is the nominal angular frequency, $\omega_{\rm c}$ is the cutoff frequency and set as 10 rad/s, respectively.

Note that in Mode I/II, since the maximum active power is delivered through two specific phases to a single-phase locomotive load, the active power in the three-phase LV side has an oscillating part at twice the grid frequency, thereby resulting in DC voltage ripples. The power reference produced by the DC-link voltage controller contains the oscillating part. This leads to the distorted grid current reference and causes additional harmonic currents. Thus, for the cancellation of the oscillating part of the power reference, a notch filter tuned at twice the grid frequency is introduced and its expression is obtained by,

$$F(s) = \frac{s^2 + \omega^2}{s^2 + 2\xi\omega s + \omega^2} \tag{31}$$

where ξ is a damping radio and is set as $\xi = 0.707$.

Figure 5 presents the block diagram of the proposed IPC strategy. The control system is composed of three main parts: 1) the DC-link voltage controller in (11) that controls the DC-link voltage so that the average value follows its reference; 2) the current reference generation in (24), (25) and (29) that generates the corresponding per-unit current reference synchronized with the grid voltage to transfer maximum active power in different modes; 3) the current controller in (30) that

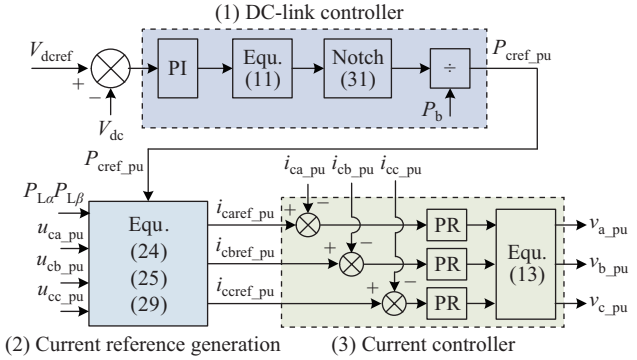


Fig. 5. Block diagram of the proposed IPC strategy.

controls the output current to track its reference with high accuracy.

For the PV application, the DC/AC converter regulates the output current with zero steady-state error and maintains a constant DC-link voltage, which are similar to the typical dual-loop schemes in [20], [21]. In the current reference generation, the current reference of each phase is independently produced on the basis of the delivered power and the converter voltage. Then, together with the current reference of each phase, the three-phase asymmetrical current reference is generated in the stationary abc reference frame. It is noted that, since the current of each phase is independently controlled by PR controllers to track its reference in the stationary abc reference frame, which is similar to a scalar control scheme, the injected current of each phase is flexibly regulated as required in (24), (25) and (29). As seen, both the current reference generation and regulation are irrelevant to the positive and negative sequence components. The IPC strategy can flexibly provide the positive and negative sequence current provision without a dual sequence current regulation. In other words, the IPC strategy need not distinguish the positive and negative sequence currents in the current reference generation and feedback regulation. Compared to the dual-sequence current regulation [19]−[24], the main advantage of the IPC strategy is its simplicity and the lack of the symmetrical component extraction.

It is noted that, for powering a single-phase locomotive load, all the active power is delivered through two wires at line voltage in Mode I/II. However, in Mode III, all the active power is delivered through three wires at phase voltage. The current amplitude of Mode I/II is $\sqrt{3}$ times as much as that of Mode III. For this reason, a higher rated current of the PV converter is required, which is equal to that of the converter in the single-phase configuration. However, compared to the solution in Fig. 1, only one three-phase converter is employed instead of two single-phase converters with a simpler implementation and lower cost.

IV. Simulation Validation

In order to evaluate the performance of the proposed IPC control strategy, a simulation model with its main circuit shown in Fig. 2 is developed on Matlab/Simulink. In the tests, one equivalent converter with a rating of 5.0 MW is used to represent all PV generation units for a simple implementation In addition, since this paper is focused on the grid-connected current regulation of the rear-end DC/AC converters, the MPPT achieved by the front-end DC/DC converter can be neglected and the delivered PV power into the common DC-link is assumed to be fixed. Thus, a constant power source can be used to represent the front-end DC/DC converter for delivering the rated power of 5.0 MW. Since electrified trains are equipped with PWM rectifiers and usually operate in the unity power factor mode, the traction load can be considered as a resistive load in the tests. The other parameters are listed in Table I. In the results, all the values are given as per-unit with a based power of 5.0 MW.

TABLE I
Simulation Parameters

Parameter	Value
Grid line voltage	110 kV
MT1 turn's radio k_1	110 kV/27.5 kV
MT2 turn's radio k_2	27.5 kV/10 kV
MT3 turn's radio k_3	10 kV/310 V
DC-link voltage of converter	1000 V
Locomotive load	10 MW

Table II presents the action sequence of the simulation cases. In 0∼0.2 s, the locomotive is on an α traction arm. Then, from 0.2 s to 0.3 s, since the locomotive is in the neutral section between two traction arms, there are no load on both of the two traction arms. In 0.3∼0.5 s, the locomotive is powered by the β traction arm. For clear comparisons, two study cases are set. In Case I, the control mode is fixed at Mode III, which is always with symmetrical current injection regardless of the locomotive loads on the traction arms. In Case II, three predefined modes are switched to each other on the basis of the locomotive loads on the two traction arms, thereby resulting in flexible operations between the symmetrical and asymmetrical current injections.

TABLE II
Action Sequence of Study Cases

Parameter	Value	Study Case	
		Case I	Case II
0∼0.2 s	$P_{L\alpha} = 2.0$ p.u., $P_{L\beta} = 0$		Mode I
0.2∼0.3 s	$P_{L\alpha} = 0$, $P_{L\beta} = 0$	Mode III	Mode III
0.3∼0.5 s	$P_{L\alpha} = 0$, $P_{L\beta} = 2.0$ p.u.		Mode II

Figure 6 shows the simulation results of Case I. In this case, the converter is controlled with Mode III enabled and only injects three-phase balanced current regardless of various load conditions. All the values are given as per-unit. As seen, the three-phase voltage in the LV side remains balanced and symmetrical, which is irrelevant to locomotive load changings. It is confirmed that the proposed configuration with an inverse V/V transformer provides a three-phase balanced voltage with PV generation. Due to the symmetrical current injection of the rated values, the converter's instantaneous active and reactive powers maintain constant at 1.0 p.u. and 0.0 p.u. The DC-link voltage of the converter is constant at 1000 V. On the HV side, when the locomotive is in the neutral section, there is no load on the two traction arms. All the active and reactive powers are fed back to the grid with balanced current. If

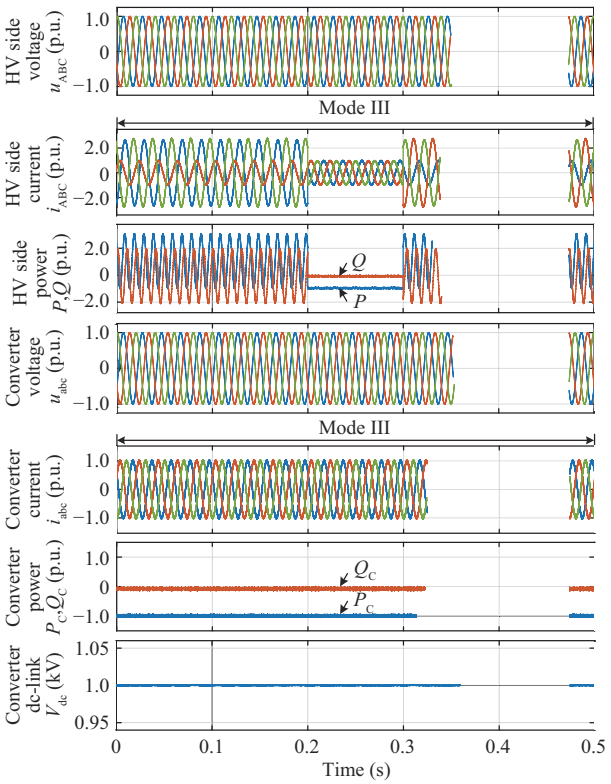


Fig. 6. Simulation results of the symmetrical current provision.

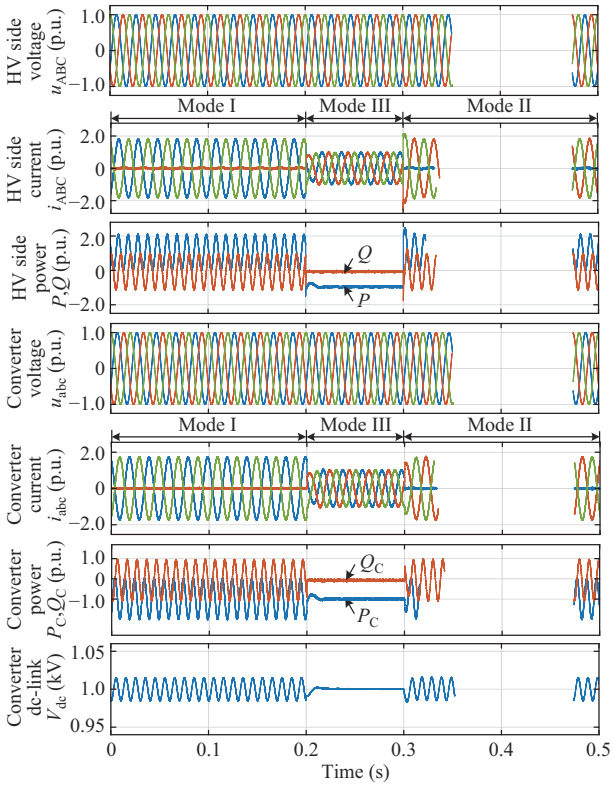


Fig. 7. Simulation results of asymmetrical and symmetrical current provisions.

there is a locomotive load of 2.0 p.u. on one traction arm, the active and reactive powers on the HV side contain ±2.0 p.u. pulsations, but the average active power on the HV side is still reduced to 1.0 p.u. due to the active power provision of PV generation. The maximum current on the HV side reaches a relatively higher amplitude of around 2.7 p.u.. This is primarily because the negative sequence current caused by the single-phase locomotive load cannot be suppressed with symmetrical current injection. Thus, the asymmetrical current injection is preferred for more negative sequence current reduction with enhanced power quality.

Figure 7 shows the simulation results of Case II. In this case, the converter is flexibly controlled to inject symmetrical and asymmetrical currents with different load conditions. When the locomotive is in the neutral section between two traction arms with no traction load, Mode III is active with symmetrical current injection. Similar to 0.2∼0.3 s in Case I, the constant active and reactive powers of 1.0 p.u. and 0.0 p.u. on the HV side are achieved with balanced currents. When the locomotive is on the α traction arm, Mode I is enabled in 0–0.2 s to deliver all the power to the locomotive with asymmetrical current injection, while Mode II is selected for the locomotive on the β traction arm in 0.3∼0.5 s. As seen, the maximum converter current reaches around 1.7 p.u., which is larger than that of Mode III. This is because all the active power is delivered through two wires with line voltages in Mode I/II, but through three wires with phase voltages in Mode III. Due to the asymmetrical current injection, the converter active power contains the oscillating part at ± 1.0 p.u., which would cause the inevitable voltage fluctuations in the common DC-link at ± 18 V. The maximum current on the HV side is decreased to around 1.7 p.u.. Compared to Case I, since asymmetrical currents are injected by supplying the partial power of the single-phase locomotive load, more NSC reduction is achieved for power quality improvement.

For clear comparisons, Table III summarizes positive-sequence current (PSC) and negative sequence current (NSC) on the HV and LV sides among different modes. The PSC on the HV side is approximately equal to each other, which is determined by the average active power of the converter and the locomotive. However, the NSC varies due to different modes. In Mode III, the NSC on the HV side is as high as 2.02 p.u.. However, in Mode I/II, the NSC on the HV side is reduced to 1.03 p.u.. This is because the converter is controlled to provide 0.99 p.u. NSC to compensate the NSC on the HV side. As a result, the proposed IPC strategy can supply the locomotive with asymmetrical current injection and then suppress the NSC on the HV sides, which can guarantee higher power quality.

TABLE III
COMPARISONS BETWEEN DIFFERENT MODES

Mode	HV side		LV side	
	PSC (p.u.)	NSC (p.u.)	PSC (p.u.)	NSC (p.u.)
Mode I/II	1.06	1.03	1.02	0.99
Mode III	1.05	2.02	1.02	0.00

V. CONCLUSION

This paper proposes the three-phase integrated configuration and IPC control strategy for PV generation in railway TPSSs.

In this configuration, an inverse V/V transformer is used to convert the two-phase traction network to a three-phase balanced LV AC bus. It is more convenient for the access of conventional three-phase PV converters. Then, for mitigating the NSC on the HV sides caused by the locomotive load, the IPC control strategy is proposed with a flexible current provision. It can not only supply the locomotive load with asymmetrical current but also feed back to the grid with symmetrical current. In this proposed strategy, the current references of each phase are used to replace those of positive and negative sequence components. All the calculations and implementations are in the stationary reference frame without sequence extracting and power compensation. Finally, simulation results are given to validate the three-phase integrated configuration and the IPC control strategy.

REFERENCES

[1] P. Cheng, H. Kong, J. Ma and L. Jial, "Overview of resilient traction power supply systems in railways with interconnected microgrid," *CSEE Journal of Power and Energy Systems*, vol. 7, no. 5, pp. 1122–1132, Sep. 2021.

[2] J. Q. Liu and J. H. Tian, "Traffic management and energy optimization for high-speed trains: an overview of methods for saving energy," *IEEE Electrification Magazine*, vol. 7, no. 3, pp. 66–75, Sept. 2019.

[3] International Energy Agency (IEA), "The future of rail: Opportunities for energy and the environment," International Energy Agency, Feb. 2019.

[4] L. Jia, J. Ma, P. Cheng and Y. Liu, "A perspective on solar energy-powered road and rail transportation in China," *CSEE Journal of Power and Energy Systems*, vol. 6, no. 4, pp. 760–771, Dec. 2020.

[5] M. Brenna, F. Foiadelli, and H. J. Kaleybar, "The evolution of railway power supply systems toward smart microgrids: the concept of the energy hub and integration of distributed energy resources," *IEEE Electrification Magazine*, vol. 8, no. 1, pp. 12–23, Mar. 2020.

[6] B. J. Yoo, C. B. Park, and J. Lee, "A study on design of photovoltaic system using electrical railway stations," in *2016 19th International Conference on Electrical Machines and Systems*, Chiba, Japan, 2016, pp. 1–5.

[7] Riding Sunbeams Ltd, "Riding sunbeams report final," 2017, pp. 9–11.

[8] JR-East Group, "CSR Report 2017: aiming for a sustainable society" (JR-East Group, 2017), pp. 110.

[9] S. D'Arco, L. Piegari, and P. Tricoli, "Comparative analysis of topologies to integrate photovoltaic sources in the feeder stations of AC railways," *IEEE Transactions on Transportation Electrification*, vol. 4, no. 4, pp. 951–960, Dec. 2018.

[10] E. P. de la Fuente, S. K. Mazumder, and I. González-Franco, "Railway electrical smart grids: an introduction to next-generation railway power systems and their operation," *IEEE Electrification Magazine*, vol. 2, no. 3, pp. 49–55, Sept. 2014.

[11] M. L. Wu, W. Y. Wang, W. L. Deng, H. B. Chen, C. H. Dai, and W. R. Chen, "Back-to-back PV generation system for electrified railway and its control strategy," in *2017 IEEE Transportation Electrification Conference and Expo, Asia-Pacific*, Harbin, China, 2017, pp. 1–6.

[12] M. L. Wu, C. H. Dai, W. L. Deng, Y. Gao, H. B. Chen, and W. R. Chen, "Back-to-back PV generation system and its control strategy for electrified railway", *Power System Technology*, vol. 42, no. 2, pp. 541–547, Feb. 2018.

[13] M. A. Shuvra and B. Chowdhury, "Distributed dynamic grid support using smart PV inverters during unbalanced grid faults," *IET Renewable Power Generation*, vol. 13, no. 4, pp. 598–608, Mar. 2019.

[14] K. Ma, L. Fang and W. Kong, "Review of distribution network phase unbalance: Scale, causes, consequences, solutions, and future research directions," *CSEE Journal of Power and Energy Systems*, vol. 6, no. 3, pp. 479–488, Sep. 2020

[15] S. Biricik and H. Komurcugil, "Three-level hysteresis current control strategy for three-phase four-switch shunt active filters," *IET Power Electronics*, vol. 9, no. 8, pp. 1732–1740, Jun. 2016.

[16] D. Sun, X. H. Wang, H. Nian, and Z. Q. Zhu, "A sliding-mode direct power control strategy for DFIG under both balanced and unbalanced grid conditions using extended active power," *IEEE Transactions on Power Electronics*, vol. 33, no. 2, pp. 1313–1322, Feb. 2018.

[17] D. H. Zhou, P. F. Tu, and Y. Tang, "Multivector model predictive power control of three-phase rectifiers with reduced power ripples under nonideal grid conditions," *IEEE Transactions on Industrial Electronics*, vol. 65, no. 9, pp. 6850–6859, Sept. 2018.

[18] N. Kumar, T. K. Saha, and J. Dey, "Control, implementation, and analysis of a dual two-level photovoltaic inverter based on modified proportional-resonant controller," *IET Renewable Power Generation*, vol. 12, no. 5, pp. 598–604, Apr. 2018.

[19] M. G. Taul, X. F. Wang, P. Davari, and F. Blaabjerg, "Current reference generation based on next-generation grid code requirements of grid-tied converters during asymmetrical faults," *IEEE Journal of Emerging and Selected Topics in Power Electronics*, vol. 8, no. 4, pp. 3784–3797, Dec. 2020, doi: 10.1109/JESTPE.2019.2931726.

[20] Y. C. Zhang, J. Jiao, J. Liu, and J. H. Gao, "Direct power control of PWM rectifier with feedforward compensation of DC-bus voltage ripple under unbalanced grid conditions," *IEEE Transactions on Industry Applications*, vol. 55, no. 3, pp. 2890–2901, May/Jun. 2019.

[21] S. F. Zarei, H. Mokhtari, M. A. Ghasemi, S. Peyghami, P. Davari, and F. Blaabjerg, "Control of grid-following inverters under unbalanced grid conditions," *IEEE Transactions on Energy Conversion*, vol. 35, no. 1, pp. 184–192, Mar. 2020.

[22] H. Nian, Y. B. Shen, H. Y. Yang, and Y. Quan, "Flexible grid connection technique of voltage-source inverter under unbalanced grid conditions based on direct power control," *IEEE Transactions on Industry Applications*, vol. 51, no. 5, pp. 4041–4050, Sept./Oct. 2015.

[23] J. D. Jia, G. Y. Yang, and A. H. Nielsen, "A review on grid-connected converter control for short-circuit power provision under grid unbalanced faults," *IEEE Transactions on Power Delivery*, vol. 33, no. 2, pp. 649–661, Apr. 2018.

[24] X. Q. Guo, W. Z. Liu, and Z. G. Lu, "Flexible power regulation and current-limited control of the grid-connected inverter under unbalanced grid voltage faults," *IEEE Transactions on Industrial Electronics*, vol. 64, no. 9, pp. 7425–7432, Sept. 2017.



Peng Cheng (M'18) received the B.S. and Ph.D. degrees from Zhejiang University, Hangzhou, China, in 2011 and 2016, both in Electrical Engineering. He is currently an Assistant Professor in the Department of China Institute of Energy and Transport Integration Development, North China Electric Power University, China.

His current research interests include renewable energy-integrated transportation, and multi-converter power systems.



Huiwen Kong received the B.S. and M.S. degrees in North China University of Water Resources and Electric Power and Zhengzhou University, China, in 2016 and 2019, respectively. She is currently working toward the Ph.D. degree in the Department of China Institute of Energy and Transport Integration Development, North China Electric Power University, China.

Her current research interests include renewable energy-integrated transportation, and grid connected control of new energy power generation.



Chao Wu (M'19) received the B.Eng. degree from Hefei University of Technology, Hefei, China and the Ph.D. degree from Zhejiang University, Hangzhou, China, in 2014 and 2019, both in Electrical Engineering. From 2019 to 2021, he was a Postdoctoral Researcher in the Department of Energy Technology, Aalborg University, Aalborg, Denmark. He is currently an Assistant Professor in the Department of Electrical Engineering, Shanghai Jiao Tong University, Shanghai, China.

His current research interests include modeling, control, and stability analysis of power electronics in renewable energy applications, particularly the control and operation of doubly fed induction generators for DC connection and the transient stability of power converters. He has published more than 20 IEEE/IET Transaction papers.



Jing Ma received the B.S. and Ph.D. degree from North China Electric Power University, China, in 2003 and 2008, respectively. He has been a visiting research scholar in the Bradley Department of Electrical and Computer Engineering, Virginia Polytechnic Institute and State University from 2008 to 2009.

He is currently a full Professor in the, North China Electric Power University, China. His major interests include renewable power generation, and power system modeling, diagnoses and protection.